



Variability of Tropical Cyclone Track Density in the North Atlantic: Observations and High-Resolution Simulations*

WEI MEI AND SHANG-PING XIE

Scripps Institution of Oceanography, University of California, San Diego, La Jolla, California

MING ZHAO

NOAA/Geophysical Fluid Dynamics Laboratory, Princeton, New Jersey, and University Corporation for Atmospheric Research, Boulder, Colorado

(Manuscript received 20 September 2013, in final form 7 March 2014)

ABSTRACT

Interannual–decadal variability of tropical cyclone (TC) track density over the North Atlantic (NA) between 1979 and 2008 is studied using observations and simulations with a 25-km-resolution version of the High Resolution Atmospheric Model (HiRAM) forced by observed sea surface temperatures (SSTs). The variability on decadal and interannual time scales is examined separately. On both time scales, a basinwide mode dominates, with the time series being related to variations in seasonal TC counts. On decadal time scales, this mode relates to SST contrasts between the tropical NA and the tropical northeast Pacific as well as the tropical South Atlantic, whereas on interannual time scales it is controlled by SSTs over the central–eastern equatorial Pacific and those over the tropical NA. The temporal evolution of the spatial distribution of track density is further investigated by normalizing the track density with seasonal TC counts. On decadal time scales, two modes emerge: one is an oscillation between track density over the U.S. East Coast and midlatitude ocean and that over the Gulf of Mexico and the Caribbean Sea and the other oscillates between low and middle latitudes. They might be driven by the preceding winter North Atlantic Oscillation and concurrent Atlantic meridional mode, respectively. On interannual time scales, two similar modes are present in observations but are not well separated in HIRAM simulations. Finally, the internal variability and predictability of TC track density are explored and discussed using HIRAM ensemble simulations. The results suggest that basinwide total TC counts/days are much more predictable than local TC occurrence, posing a serious challenge to the prediction and projection of regional TC threats, especially the U.S. landfall hurricanes.

1. Introduction

Tropical cyclones (TCs) are among the most devastating weather events on Earth with extremely important societal impacts (e.g., Pielke and Landsea 1998; Pielke et al. 2008). In addition, these powerful storms potentially play important roles in the climate system by

affecting heat transport (Emanuel 2001; Srivier and Huber 2007; Korty et al. 2008; Mei et al. 2013). An adequate understanding of TC variability and the underlying mechanisms helps to improve the accuracy of seasonal predictions and long-term projections of TC activity, which in turn helps the community to be better prepared for TC-imposed threats. Research in this field has received much attention because of the strong rise of TC activity in the North Atlantic (NA) starting in the mid-1990s (e.g., Goldenberg et al. 2001; Holland and Webster 2007; Klotzbach and Gray 2008).

There are several measures of TC activity, including genesis; counts; intensity; tracks; and some other derivatives, such as the power dissipation index (PDI;

* Supplemental information related to this paper is available at the Journals Online website: <http://dx.doi.org/10.1175/JCLI-D-13-00587.s1>.

Corresponding author address: Wei Mei, Scripps Institution of Oceanography, University of California, San Diego, 9500 Gilman Drive #0206, La Jolla, CA 92093-0206.
E-mail: wmei@ucsd.edu

Emanuel 2005a) and the accumulated cyclone energy (ACE; Bell et al. 2000). Our focus here is on interannual–decadal variability of seasonal TC track density. The seasonal track density can be considered as a combination of seasonal TC counts, spatial distribution of TC genesis, and subsequent tracks, but it has not received enough attention as its three contributors.

Numerous studies have shown that, in the NA, TC genesis and the associated seasonal TC counts, to a large extent, are controlled by their large-scale environment: favorable conditions include above-normal rainfall over the Sahel region of West Africa and below-normal sea level pressure (SLP), above-normal low-level vorticity, and below-normal vertical wind shear over the subtropical NA (e.g., Ballenzweig 1959; McBride and Zehr 1981; Landsea and Gray 1992; Goldenberg and Shapiro 1996; Knaff 1997; Landsea et al. 1999; DeMaria et al. 2001; Nolan and Rappin 2008; Fink et al. 2010; Daloz et al. 2012). In addition, smaller-scale thermodynamics and TC internal dynamics also play an important role in TC genesis (e.g., Simpson et al. 1997; Raymond and Sessions 2007; Wang 2012; Smith and Montgomery 2012; Komaromi 2013) and thus modulate TC counts. On the other hand, TC tracks are primarily determined by environmental steering flows with a relatively smaller contribution from the interaction between TC dynamics and the steering flow (e.g., George and Gray 1976; Holland 1983). They are identified to exhibit strong intrabasin variabilities in the NA and much of them can be connected to various climate modes, such as the El Niño–Southern Oscillation (ENSO) and the North Atlantic Oscillation (NAO) (Elsner et al. 2000; Elsner 2003; Kossin et al. 2010).

The large-scale factors affecting TC genesis and tracks are not necessarily the same, although TCs generated in different regions have, on average, different flavors for their paths (straight moving versus recurving; e.g., Wang et al. 2011; Colbert and Soden 2012). Accordingly, we expect to see a strong modulation of TC track density by large-scale ambient conditions and various modes of climate variability but not necessarily in a way the same as the modulation of TC genesis and/or TC tracks. This complicates an understanding of the variability in TC track density, which is more directly linked to societal and economic impacts of TCs (e.g., landfall).

To our knowledge, Xie et al. (2005b) are among the first investigating the variability of NA TC track density. By means of principal component analysis, they depict three distinct modes of TC track density and connect each of them to different climate modes including ENSO, the dipole mode of Atlantic sea surface temperature (SST), the NAO, and the Arctic Oscillation. More recently, although they do not directly address

track density, Kossin et al. (2010) perform a thorough study of NA TC tracks. Specifically, they separate the tracks into four groups, study the respective variabilities in the frequency of different groups on various time scales, and understand their connections to the Madden–Julian oscillation in addition to the climate modes examined in Xie et al. (2005b). The findings presented in these studies have advanced our knowledge of climate controls of the preferred TC track pattern and provided valuable information regarding predicting and projecting the frequency of TCs striking the East Coast and Gulf Coast of the United States.

The analysis by Xie et al. (2005b) is, however, for a limited domain (i.e., 50°–86°W, 20°–50°N) that excludes the Caribbean Sea and the main development region (MDR) of NA TCs and most of the Gulf of Mexico, and it only focuses on TCs of hurricane intensity. On the other hand, the primary interest of Kossin et al. (2010) lies in TC tracks whose spatiotemporal variabilities may differ from TC track density that more directly relates to the TC-induced damage to human society. Here we extend the study area of Xie et al. (2005b) to the whole NA basin and systematically explore interannual–decadal variability of the NA TC track density and the associated climate modes. The results will also be compared with some of the findings in Kossin et al. (2010) that are based on an alternative method: cluster analysis. More importantly, our observational analysis is aided by an ensemble simulation of a global high-resolution atmospheric model, which can well capture the observed variability in NA seasonal TC counts when forced by observed SSTs. Comparisons between the observed and simulated variability would shed light on whether and the extent to which the variation of TC track density may be explained by SST variability, with important implications for predictability. We also for the first time explore internal variability in the NA TC track density using high-resolution ensemble simulations, which has important implications regarding the predictability of local TC occurrence as well.

After presenting the data and methods in use (section 2), we evaluate the general performance of the high-resolution model in reproducing global TC climatologies (including seasonal TC counts and their variations from basin to basin) and temporal variability of seasonal TC counts as well as spatial distribution of climatological TC track density over the NA (section 3). We then explore respectively low- and high-frequency variability of NA TC track density and the corresponding underlying mechanisms in sections 4 and 5. The internal variability and predictability of NA TC track density are examined and discussed in section 6.

2. Data and methods

a. Observed TC tracks

The observed TC tracks are from the National Hurricane Center best-track dataset (McAdie et al. 2009), which provides the location and intensity of TCs in the North Atlantic at 6-h intervals. The observations are available since 1851 but, to be consistent with the availability of the model output described below, only the observed track data between 1979 and 2008 are used.

b. Simulated TC tracks

We use output from a 25-km-resolution version of the High Resolution Atmospheric Model (HiRAM) to study the variability of TC activity in response to observed SSTs. We note that Emanuel and Sobel (2013) recently suggested that climate model simulations forced only with observed SSTs may not produce correct surface fluxes and correct surface wind speeds and may thereby influence TC-related thermodynamic parameters and eventually TC activity, particularly potential intensity. This effect on some TC metrics, such as TC number and TC tracks that we are interested in this study, however, may be not that important. Indeed, a 50-km-resolution version of HiRAM has been shown to well simulate the observed climatology and interannual variability of hurricane numbers in various basins when forced by observed SSTs (Zhao et al. 2009). A detailed description of HiRAM can be found in Zhao et al. (2012).

This study uses 6-h fields including SLP, 850-hPa vorticity, temperature averaged between 300 and 500 hPa, and near-surface winds to detect and track TCs following the methodology modified from Knutson et al. (2007) and Zhao et al. (2009). Specifically, we first identify potential storms based on the following criteria:

- 1) The 850-hPa relative vorticity maxima exceeding $3.2 \times 10^{-4} \text{ s}^{-1}$ are located within areas of $4.5^\circ \times 4.5^\circ$ latitude and longitude.
- 2) The local minimum of SLP, which must be within a distance of 2° latitude or longitude from the 850-hPa relative vorticity maximum, is defined as the center of the storm and should be at least 6 hPa lower than the environment. The local maximum surface (lowest model level) wind speed within an area of 2.6° latitude and longitude is detected to represent the intensity of the storm.
- 3) The local maximum of 300–500-hPa averaged temperature is defined as the center of the warm core. Its distance from the storm center must be within 2° latitude or longitude, and its temperature must be at least 1°C warmer than the environment.

After identifying all potential storm snapshots, a trajectory analysis is then carried out to find TC tracks. The qualified tracks must meet the following conditions:

- 1) The distance between two consecutive snapshots (with a time interval of 6 h) must be shorter than 400 km.
- 2) The track must last longer than 4 days, and the maximum surface wind speed is greater than 17.5 m s^{-1} during the life cycle of the TC.

Slight changes in the above-mentioned conditions do not significantly change the results presented below.

The model solutions are sensitive to initial conditions because of the chaotic and nonlinear nature of atmospheric processes (e.g., Harzallah and Sadourny 1995; Griffies and Bryan 1997). Accordingly, the simulated TC activity is also sensitive to initial conditions as confirmed by Zhao et al. (2009), who show that simulations initialized with slightly different conditions produce significant differences in the simulated interannual variation of basin-wide hurricane counts. To extract a reproducible signal associated with the external forcing (i.e., observed SSTs), we use three-member ensemble simulations that are different only in initial conditions. The ensemble mean is considered as the forced response to the prescribed SSTs from observations. The deviation of each member from the ensemble mean represents internal variability of the model. To further advance our understanding of the internal variability, we also use TC tracks detected from the output of a 50-km-resolution version HiRAM that is forced by repeating seasonally varying climatological SSTs and fixed atmospheric radiative gases for 20 yr. The 20 yr of data can be considered as 20 members that are different in initial conditions but subject to the same SST forcing (i.e., observed monthly climatological SSTs).

c. Methods

TC track density on a yearly basis for both observations and simulations are calculated as the duration of TC tracks within each $8^\circ \times 8^\circ$ grid within the study area of 108°W – 0° and 0° – 50°N during the NA hurricane season (i.e., 1 June–30 November). (We use this large grid to reduce the noise level; using a smaller grid, such as $5^\circ \times 5^\circ$ or $6^\circ \times 6^\circ$, gives similar results.) The leading modes of variability in TC track density are extracted using an empirical orthogonal function (EOF) analysis. Linear correlation and regression analyses are applied to identify the SST pattern(s) and atmospheric conditions responsible for each individual leading mode of the TC track density. The global mean SST (averaged between 65°S and 65°N) is removed before calculating the correlation and performing the regression analysis. Without this removal procedure, similar results are obtained.

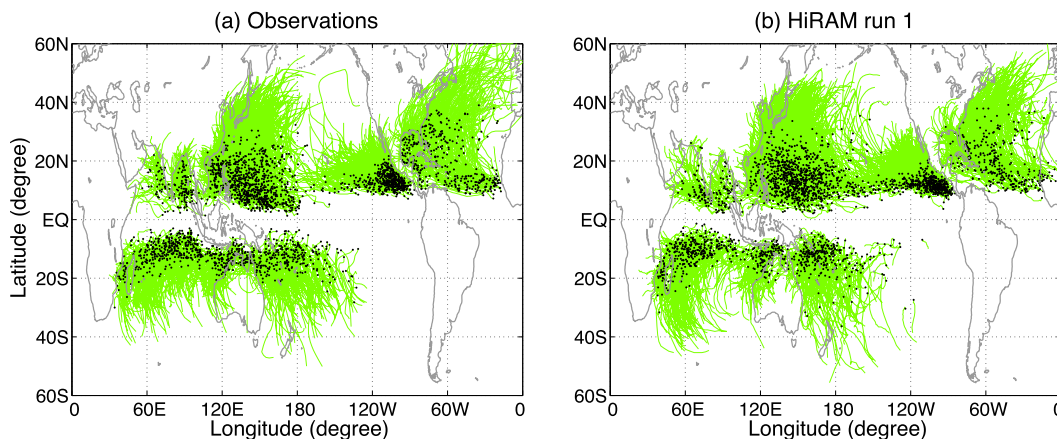


FIG. 1. Global TC genesis (black dots) and tracks (green curves) between 1979 and 2008 from (a) observations and (b) one realization using the 25-km-resolution version of HiRAM. Note that several TCs over the South Atlantic and medicanes over the Mediterranean Sea (e.g., Emanuel 2005b) are not shown.

3. General performance of HiRAM

Figure 1 shows the geographical distribution of TC genesis and tracks for 1979–2008 from observations and one HiRAM simulation. Generally, HiRAM reproduces the spatial distribution of TC genesis in observations, such as high genesis density in both the western and eastern North Pacific and relatively sparse genesis density over the NA. The simulated tracks also closely resemble those from observations; for example, the model can capture the poleward extension of observed tracks: larger poleward extension of tracks in both the western North Pacific and the NA than in the eastern North Pacific. However, there are notable discrepancies, including too few TCs in the model over the Gulf of Mexico and South China Sea compared to observations.

The simulated climatological TC numbers in each individual basin (i.e., the NA, the eastern North Pacific, the western North Pacific, the north Indian Ocean, the south Indian Ocean, and the western South Pacific) are quite close to the observed ones, with the western North Pacific having more TCs than any other basins and the north Indian Ocean experiencing the smallest number of TCs (Fig. 2).

The interannual variation in TC counts is also simulated with some degree of fidelity, particularly in the NA, consistent with Zhao et al. (2009). Figure 3 shows that the variability on both decadal and interannual time scales of observed TC and hurricane counts is well captured by the model. The large deviation of the simulations from the observations during the first few years may be due to the inaccuracy in the observed SSTs before the availability of satellite measurements (Rayner et al. 2003).

Figure 4 compares the observed and simulated spatial distribution of climatological TC track density during the

NA hurricane season. Generally, HiRAM captures the observed large-scale pattern and magnitude of the track density. For instance, both the simulated and observed track density is concentrated between 15° and 35°N with the highest density around 4 days yr⁻¹. However, large discrepancies exist over regions around 25°N: too sparse over the Gulf of Mexico while too dense over the open ocean.

4. Low-frequency variability

TC activity in the NA exhibits strong variability on both decadal and interannual time scales (e.g., Landsea

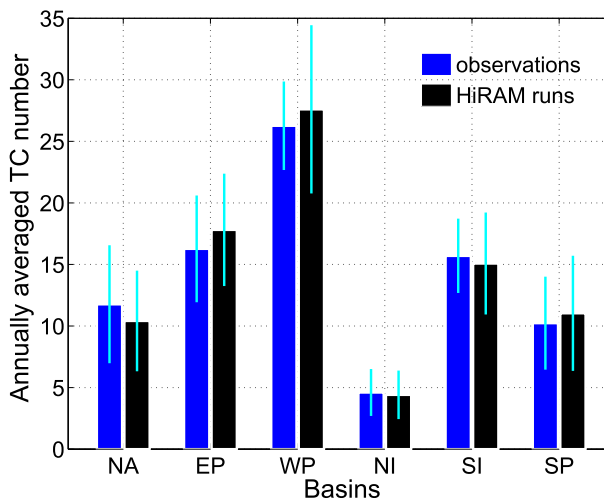


FIG. 2. A comparison of observed (blue bars) and simulated (black bars) climatological TC numbers (averaged between 1979 and 2008) in different basins: NA, eastern North Pacific (EP), western North Pacific (WP), north Indian Ocean (NI), south Indian Ocean (SI), and western South Pacific (SP). Thin cyan vertical lines indicate the standard deviation of TC numbers during the study period.

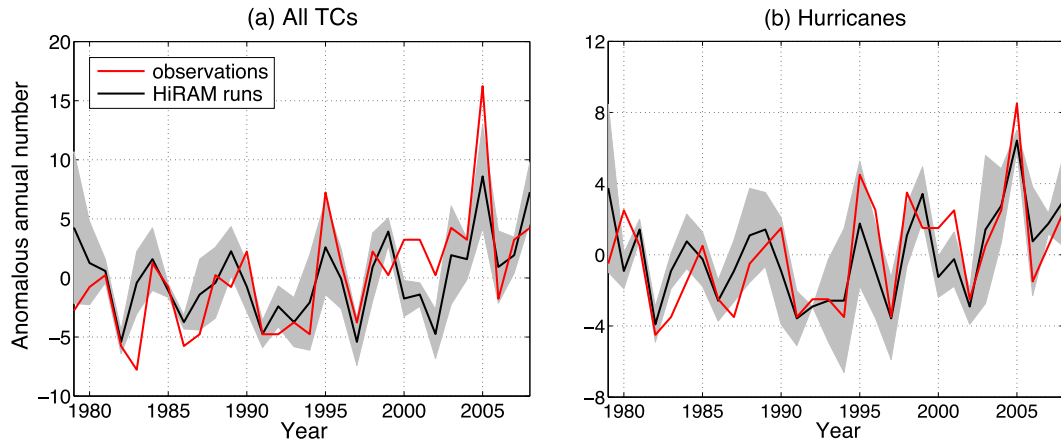


FIG. 3. A comparison of observed (red curve) and simulated (black curve) anomalies in the number of (a) TCs and (b) hurricanes in the NA between 1979 and 2008. The gray shading shows the spread of the model results, represented by the standard deviation of the results from the three ensemble members.

et al. 1999; Vitart and Anderson 2001; Bell and Chelliah 2006). In this study, we separate out these time scales and explore the two components individually. We obtain the low-frequency component using a 7.5-yr low-pass filter based on the fast Fourier transform (FFT) technique. We tested the results using a 10-yr low-pass filter and obtained very similar results. To have a slightly larger degree of freedom for the low-frequency component (considering the 30-yr period of the simulations), we chose to use the 7.5-yr low-pass filter.

EOF analysis is applied to both observed and modeled TC track density after the low-pass filtering. In both observations and model simulations, the low-frequency TC track density is dominated by a basinwide mode (mode L1; Figs. 5a,b), indicating that on decadal time scales TC track density varies simultaneously over the whole NA basin. The corresponding time series [i.e., the principal component (PC); Fig. 5d] shows that during

the first half of the study period the TC track density was suppressed while it was active during the later period. The transition occurred in the mid-1990s, consistent with the findings that the NA TC activity has strengthened since that time. The phase is consistent with the Atlantic multidecadal oscillation (AMO; e.g., Goldenberg et al. 2001). And in both observations and simulations, the PC of the low-frequency track density almost overlaps with the time series of the corresponding normalized low-frequency TC counts (Fig. 5d), indicating that this basinwide mode is largely controlled by variations in seasonal TC counts.

The loading over the Gulf of Mexico is significantly underestimated in model simulations (cf. Figs. 5a,b), consistent with the underestimated climatology of TC track density discussed before (Fig. 4). To remedy this, we scale the modeled TC track density at each grid by its corresponding observed climatology so that the

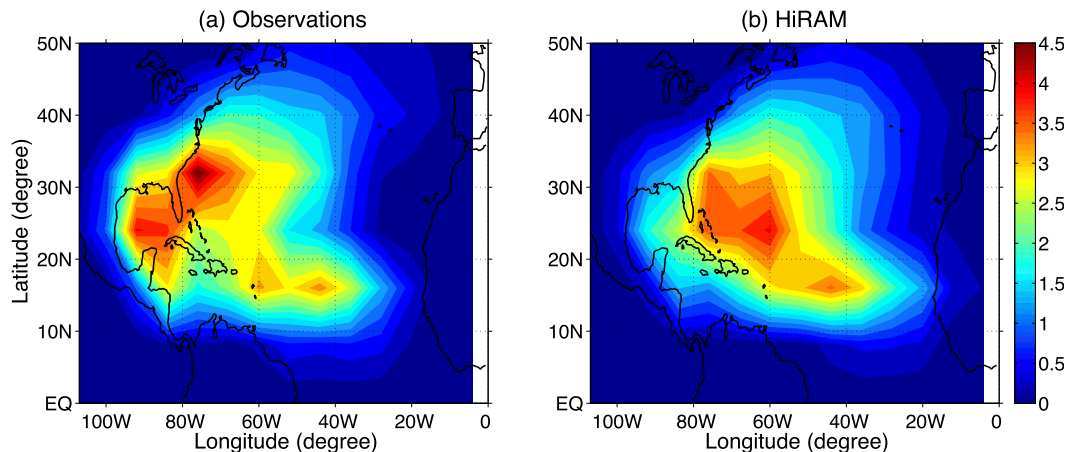


FIG. 4. (a) Observed and (b) simulated geographical distribution of the climatological TC track density (days yr^{-1}) during the NA hurricane season calculated at each $8^\circ \times 8^\circ$ grid.

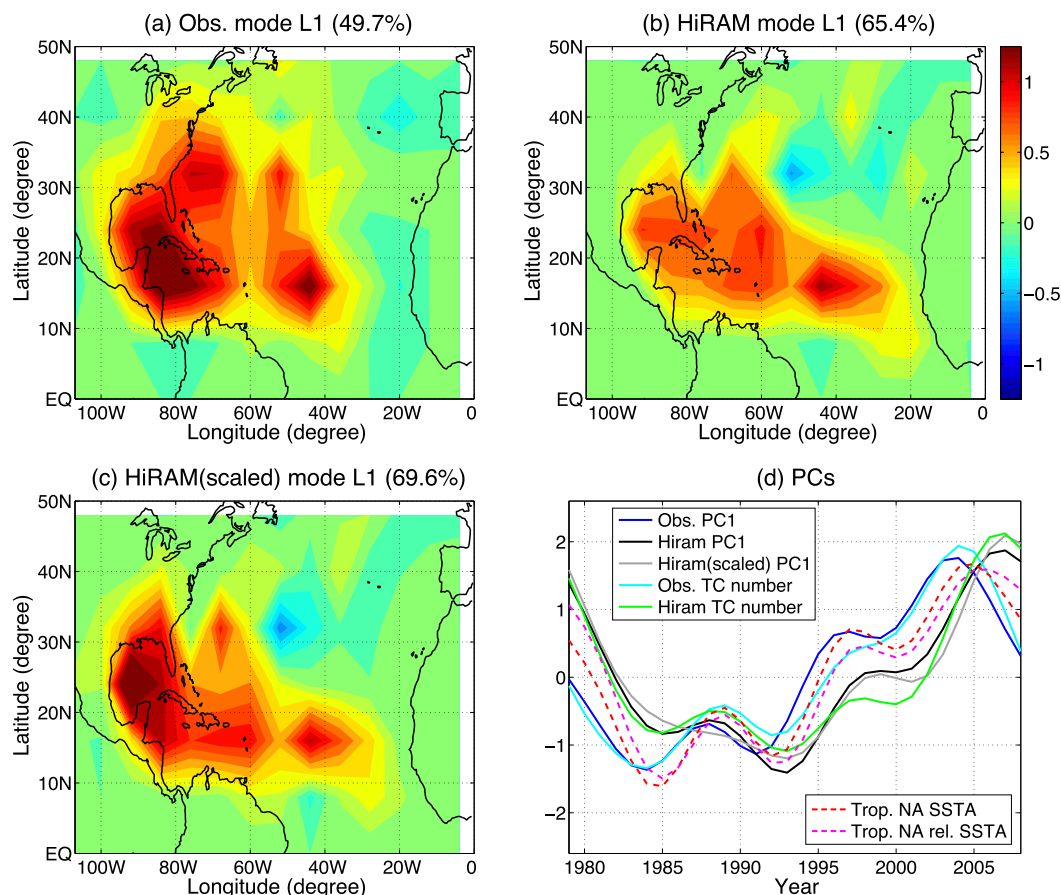


FIG. 5. (a) Spatial pattern of the first leading mode of the low-pass-filtered observed TC track density (mode L1; days yr^{-1}) in the NA during the hurricane season. (b) As in (a), but for the simulated track density. (c) As in (b), but for the simulated track density normalized by the ratio of simulated climatology to observed climatology. (d) The corresponding normalized time series together with the normalized low-frequency anomalies in seasonal TC counts from both observations and simulations as well as normalized low-frequency anomalies in the area-mean absolute SST over the tropical NA and its value relative to the global tropical mean SST.

simulations have the same climatology as the observations. Then the scaled field is subject to EOF analysis after removing high-frequency variability. The spatial pattern of the dominant mode is shown in Fig. 5c. It is clear that after the scaling, the pattern and magnitude get closer to the observations, while the PC of the simulated TC track density remains largely unchanged.

The reader may question the validity of the results since the data in use are only 30-yr long and may not be long enough to study decadal variability and the loadings may be dominated by the trend over this short study period. Indeed, the linear trend of the TC track density shows a spatial pattern similar to that of mode L1 shown above (Fig. S1 in the supplemental material), and the loading of mode 1 of the low-frequency track density with the linear trend removed prior to EOF analysis is significantly reduced over most of the NA (except over the Gulf of Mexico; Fig. S2 in the supplemental

material). However, when we repeated the EOF analysis using the observed TC best-track data between 1950 and 2009 (i.e., a doubled length), the obtained modes are insensitive to whether the linear trend is removed (Fig. S3 in the supplemental material). Also, the obtained spatial pattern is nearly identical to that of mode L1 shown above in Fig. 5a, and its PC almost overlaps with the PC of mode L1 between 1979 and 2008. All these suggest that 1) the main results presented in this study are not sensitive to the length of the data and 2) the trend during the period of 1979–2008 is actually a part of the interdecadal variability over a longer time period. Because of the latter point, in this study we do not differentiate the trend over the study period (i.e., 1979–2008) from the interdecadal and low-frequency variability.

A close inspection of Fig. 5d reveals that the PCs of the simulations lag the PC of the observations by 2–3 yr. To understand this interesting point, we repeated

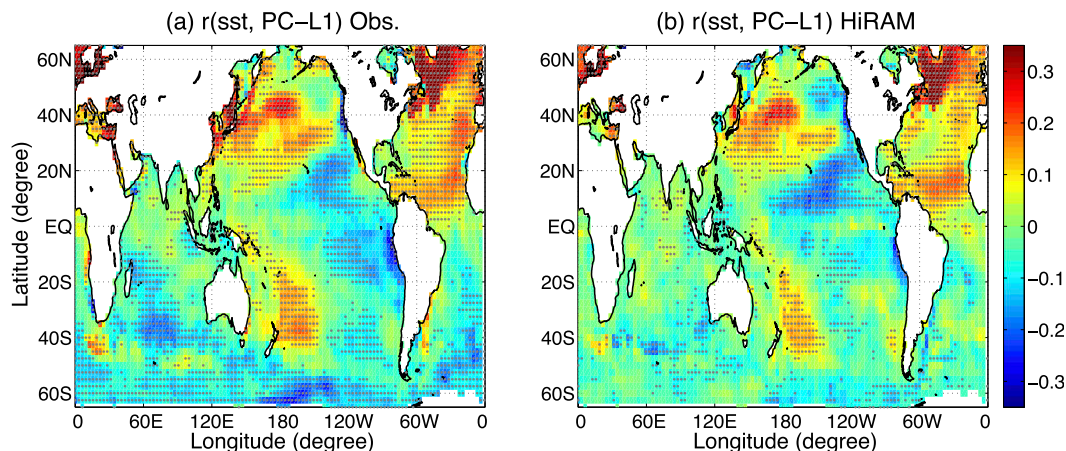


FIG. 6. Regression of the low-pass-filtered SSTA ($^{\circ}\text{C}$) onto the PC of mode L1 shown in Fig. 5 for (a) observations and (b) HiRAM simulations. Areas with a linear correlation coefficient of greater than 0.5 are stippled.

the EOF analysis using low-pass-filtered SLP fields from the National Centers for Environmental Prediction (NCEP)–U.S. Department of Energy (DOE) Reanalysis-2 (Kanamitsu et al. 2002)¹ and the HiRAM simulations. The lead–lag relation also exists in the PCs of the SLP (not shown). This provides a clue that the lag may be due to the fact that, in observations, the atmosphere modulates TC activity and the ocean simultaneously, while in the model the state of the SSTs, reflecting the state of the atmosphere in previous years, induces a response in the atmosphere that in turn affects the TC activity. This speculation merits further exploration and may be tested by comparing a coupled run and an atmosphere-only run forced by SSTs that are produced by the coupled run [i.e., following the procedure of the Atmospheric Model Intercomparison Project (AMIP)].

To understand what patterns of SST force this mode of low-frequency TC track density, we regress low-pass-filtered SST anomalies (SSTAs) onto the obtained PCs shown in Fig. 5d. In both observations and simulations (Fig. 6), a combination of two SST patterns emerges. The first is a zonal gradient in SSTs between the tropical NA and the tropical northeast Pacific, and the second pattern is a (relatively weak) meridional gradient in SSTs between the tropical NA and the tropical South Atlantic. It is worth noting that, for the first pattern, the cold SSTA in the tropical northeast Pacific may be a result of the tropical NA warming through a Rossby wave response (e.g., Zhang and

Delworth 2005; Sutton and Hodson 2007). We also plot in Fig. 5d the time series of the normalized anomaly of low-pass-filtered absolute and relative SSTs in the tropical NA. Both exhibit very similar temporal evolution as TC-related variables, indicating the key role of AMO in shaping NA TC counts and basin-integrated track density on decadal time scales (e.g., Goldenberg et al. 2001). The underlying atmospheric mechanisms relevant to these two SST patterns will be investigated later.

Previous studies have shown that there are oscillations of TC activity between different parts of the NA basin (e.g., Kimberlain and Elsner 1998; Elsner 2003; Kossin et al. 2010), which are different from the basinwide mode discussed above. To remove this basinwide mode that is tightly linked to seasonal TC counts and to extract the patterns associated with the oscillations suggested in previous studies, we normalize TC track density by seasonal total TC counts and then subject the normalized track density after low-pass filtering to EOF analysis.

Figure 7 shows the first leading mode of the normalized track density (mode LN1). Despite some discrepancies, both the observations and simulations show an oscillation of the proportion of track density between two areas: one is the U.S. East Coast and midlatitude open ocean, and the other includes the Gulf of Mexico, Caribbean Sea, and—to a lesser extent—the MDR. The corresponding PCs are shown in Fig. 7c. The proportion of TC activity over the East Coast and the midlatitude open ocean increased during the first decade, peaked in the early 1990s, and then decreased. The changes in the time series resemble the NAO index during the preceding winter season (red curve in Fig. 7c). This is consistent with Elsner et al. (2000) and

¹Using NCEP–National Center for Atmospheric Research (NCAR) Reanalysis-1 data produces nearly identical results for this and all following analyses.

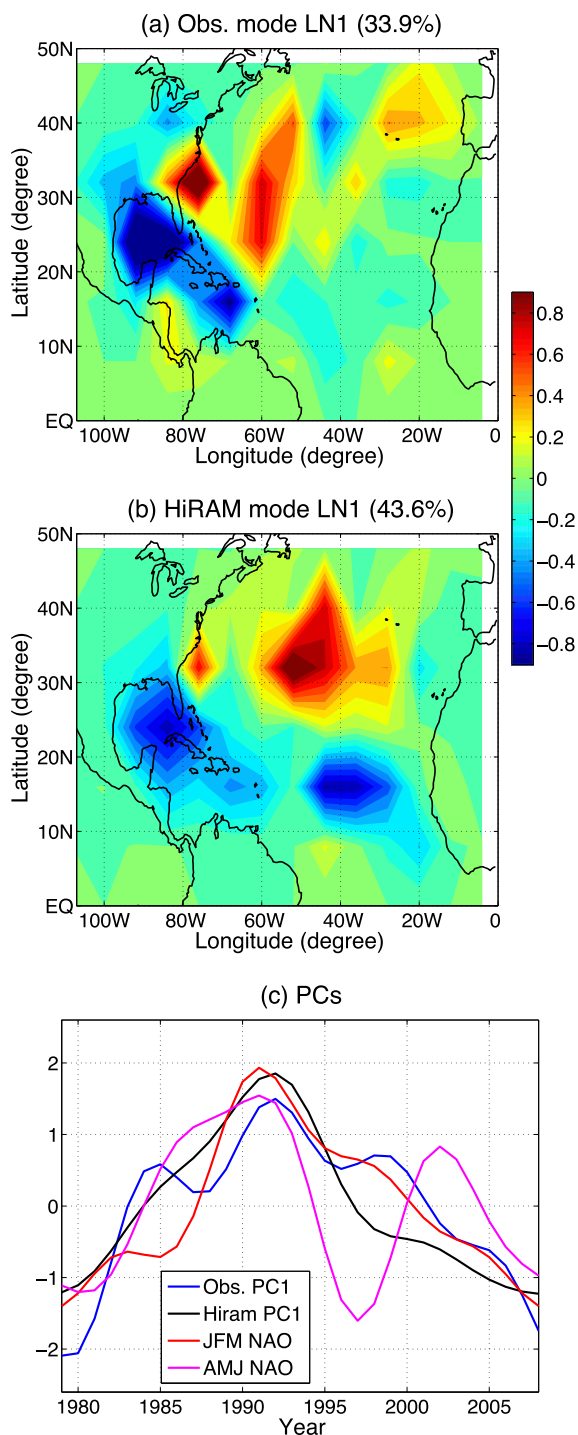


FIG. 7. (a) Spatial pattern of the first leading mode of the observed low-pass-filtered TC track density (mode LN1; days yr⁻¹) after being normalized using seasonal TC counts during the NA hurricane season. (b) As in (a), but for the simulated track density. (c) The corresponding normalized PCs for observations (blue) and simulations (black) together with the normalized low-pass-filtered NAO index averaged between January and March (red) and between April and June (magenta). (The NAO index is from www.cpc.ncep.noaa.gov/products/precip/CWlink/pna/nao_index.html.)

Elsner (2003) that TC activity in the Gulf of Mexico, to some degree, is opposite to that in the East Coast, and such an oscillation is modulated by the NAO. The minimum in the relative proportion of the Gulf of Mexico TC activity during the early 1990s is also evident in the second panel of Fig. 5 in Kossin et al. (2010). Because the NAO index is not based on SSTs while the model is forced by SSTs only, the combination of analyses of observations and simulations shown here further demonstrates the possible mechanism that the NAO phenomenon in the previous winter season forces the ocean and the resultant SSTAs then affect the atmosphere and TC activity during the hurricane season.

To understand the mechanisms responsible for mode LN1, we regress low-pass-filtered SSTAs, SLP, 850-hPa vorticity, vertical wind shear, and 500-hPa vertical pressure velocity onto the PCs shown in Fig. 7c. The SST pattern (Fig. 8a) is similar to the first SST pattern discussed before (Fig. 6); that is, opposite anomalies over the tropical NA and the tropical northeast Pacific. When the tropical NA is anomalously cold and the tropical northeast Pacific is anomalously warm, TC track density over the U.S. East Coast and the open ocean makes an above-normal contribution to basin-integrated total track density (i.e., total TC days) than that over the Gulf of Mexico and Caribbean Sea. This is concurrent with anomalously high SLP over the subtropical NA (Fig. 8b). The anomalous atmospheric circulation induces below-normal vorticity over regions extending from the Gulf of Mexico southeastward through the MDR and above-normal vorticity between 30° and 40°N (Fig. 8c). The vertical wind shear exhibits a similar pattern with a slightly southward shift (Fig. 8c). Changes in other variables, such as midtroposphere vertical velocity, show consistent changes (Fig. 8b). As suggested by Emanuel (2007) and Vimont and Kossin (2007), various climate conditions act in a consistent way to affect the NA TC activity.

The second leading mode (i.e., mode LN2) of the normalized TC track density in observations and the third leading mode (i.e., mode LN3) in simulations are characterized by an oscillation between lower latitudes (including the Caribbean Sea and MDR) and subtropics (including the Gulf of Mexico and East Coast) (Fig. 9). Note that the smaller amplitude over the Gulf of Mexico and Caribbean Sea in simulations than observations is due to the sparser climatological TC track density in simulations than observations over these regions (Fig. 4). The temporal evolution of this mode exhibits a below-normal condition and above-normal condition occurring before and after the early 1990s, respectively. The proportion of TC track density over the lower latitudes has increased since the mid-1980s. This is in accord

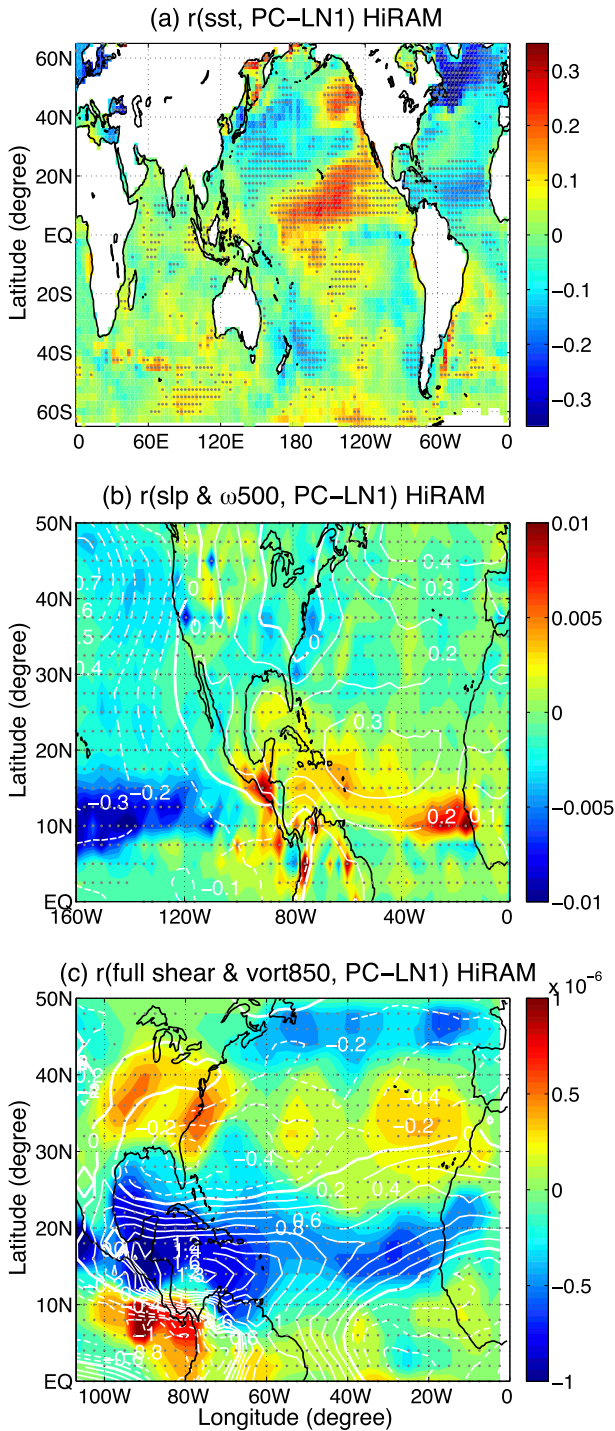


FIG. 8. Regression of (a) SSTA ($^{\circ}\text{C}$), (b) SLP (contours; hPa) and 500-hPa vertical pressure velocity (shading; Pa s^{-1}), and (c) vertical wind shear (contours; m s^{-1}) and 850-hPa vorticity (shading; s^{-1}) onto the PC of mode LN1 from simulations shown in Fig. 7. Contour interval is 0.1 hPa in (b) and 0.2 m s^{-1} in (c). Areas with correlation coefficient greater than 0.5 are stippled, and a median spatial filtering has been applied twice to the vorticity field in (c).

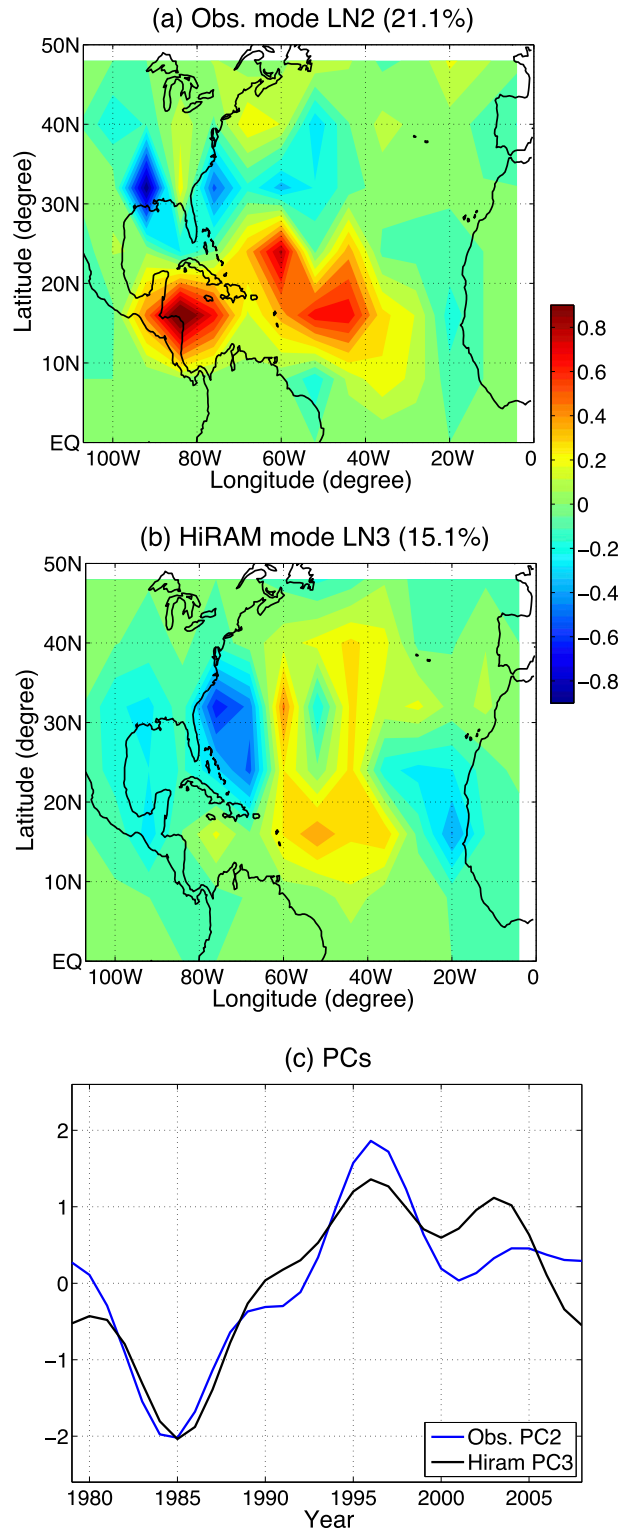


FIG. 9. As in Fig. 7, but for the second leading mode of the normalized TC track density in observations and the third leading mode in simulations (mode LN2 and mode LN3, respectively).

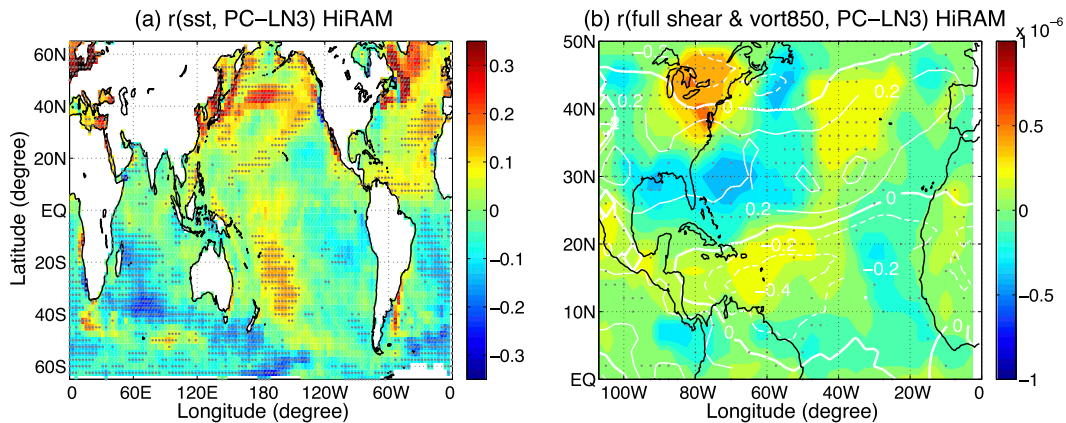


FIG. 10. Regression of (a) SSTA ($^{\circ}\text{C}$) and (b) vertical wind shear (contours; m s^{-1}) and 850-hPa vorticity (shading; s^{-1}) onto the PC of mode LN3 from simulations shown in Fig. 9. In (b), contour interval is 0.2 m s^{-1} , areas with correlation coefficient greater than 0.5 are stippled, and a median spatial filtering has been applied twice to the vorticity field.

with a recent study by Kossin et al. (2010), who identify that a regime shift occurred around the mid-1980s toward a greater proportion of lower-latitude TC activity. Figure 5 of Kossin et al. (2010) also suggests that there is a systematic shift toward proportionally more eastern NA storm tracks and proportionally fewer Gulf of Mexico storm tracks. This feature is captured by our analysis as well (Figs. 9a,b), and the PCs in Fig. 9c exhibit a similar evolution as the low-pass-filtered time series of clusters 2 and 3 in Fig. 5 of Kossin et al. (2010).

Regression of SSTA onto the time series after low-pass filtering (Fig. 10a) shows a contrast in SST between the NA and South Atlantic. This SST pattern resembles the Atlantic meridional mode, which involves cross-equatorial interactions between the ocean and atmosphere (Chang et al. 2006). The association of this climate mode and NA TC activity has been noted in previous studies (e.g., Xie et al. 2005a; Vimont and Kossin 2007; Kossin and Vimont 2007; Smirnov and Vimont 2011). Analyses of 850-hPa relative vorticity and vertical wind shear show consistent results with increased vorticity and reduced wind shear over the lower-latitude region and reduced vorticity and increased wind shear over the higher-latitude region (Fig. 10b), although the signal is generally much weaker than that for mode LN1; regression of 500-hPa vertical velocity also shows consistent results (not shown). These are consistent with the recent findings by Merlis et al. (2013) based on aquaplanet simulations and suggest that, by controlling the position and strength of the NA intertropical convergence zone (ITCZ), the meridional SST gradient between the NA and South Atlantic induces changes in atmospheric circulation and associated low-level vorticity and vertical wind shear and thereby modulates TC activity over the NA.

5. High-frequency variability

It has been known for several decades that climate modes on interannual time scales (e.g., ENSO) exert a strong control on NA TC activity (e.g., Gray 1984; Klotzbach 2011). This section examines the interannual variability of TC track density and associated dominant SST patterns. EOF analysis is applied to the 7.5-yr high-pass-filtered TC track density. Figure 11 shows the spatial pattern of the first leading mode (mode H1) and the corresponding PCs. Similar to the low-frequency track density, the first leading mode of the high-frequency track density is a basinwide mode in both observations and HiRAM simulations (Figs. 11a,b). Correcting the biases in the climatological distribution makes the simulated pattern more closely resemble the observations, particularly over the Gulf of Mexico and Caribbean Sea (Fig. 11c). The PCs for the observations and simulations are very similar with a linear correlation coefficient of around 0.78. Also, these PCs almost overlap with the time series of the normalized high-frequency seasonal TC counts (Fig. 11d), suggesting that this basinwide mode is largely controlled by variations in seasonal TC counts, as on the low-frequency time scales (Fig. 5d).

Regression of high-frequency SSTAs onto the PCs (Fig. 12a) suggests that SSTAs both in the tropical Pacific associated with ENSO and in the tropical NA force the basinwide TC activity on interannual time scales. Then it is curious to know whether the SSTAs in these two regions act independently so that the regressed pattern reflects an optimal SST pattern or they simply correlate with each other and only one of them affects TC activity. To answer this, we calculate the correlation between Niño-3.4 index (defined as the SSTA averaged over the region 170° – 120°W , 5°S – 5°N) and global

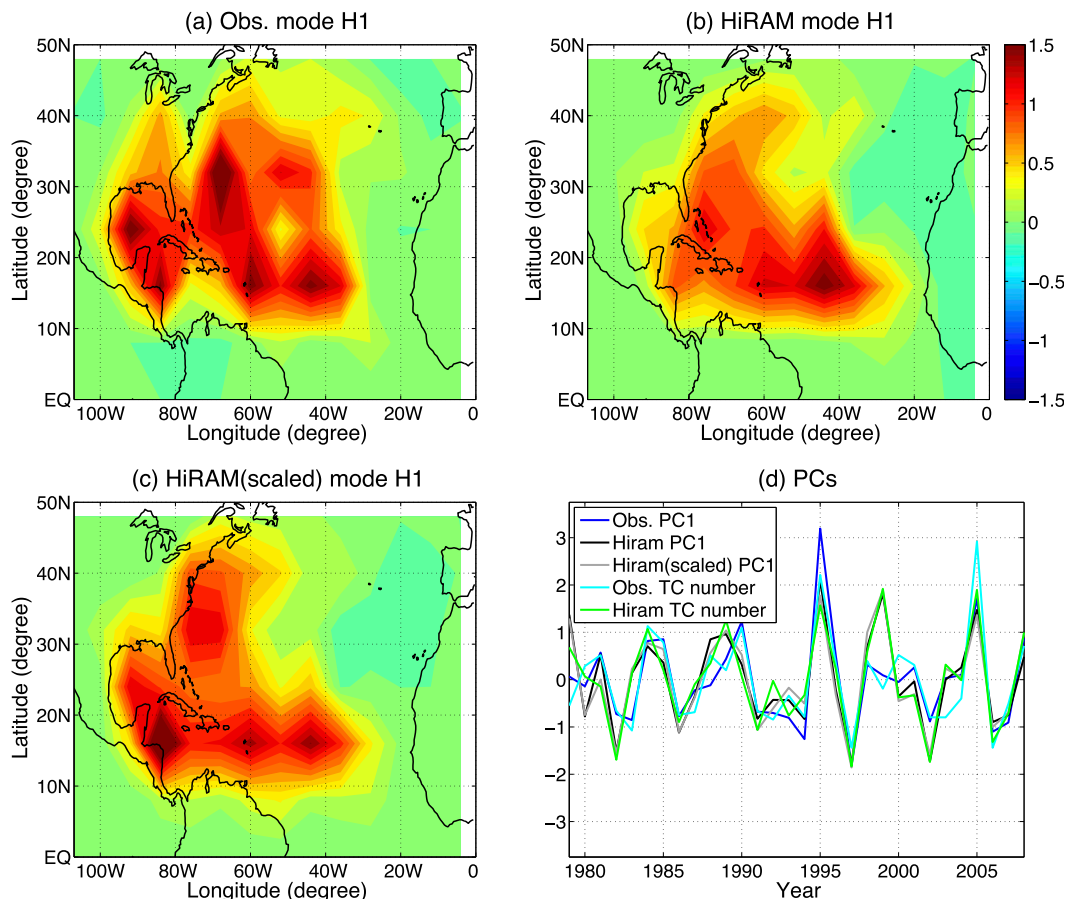


FIG. 11. As in Fig. 5, but for the first leading mode of the high-pass-filtered TC track density (mode H1).

SSTAs. As shown in Fig. 12b, SSTs in the central and eastern equatorial Pacific have no significant correlation with the simultaneous SSTs over the tropical NA during the NA hurricane season (i.e., June–November). This suggests that both ENSO and SSTAs over the tropical NA contribute to modulating the NA TC track density, and the SSTA pattern shown in Fig. 12a reflects an optimal SST pattern for an active TC season: TC activity is maximized when the SST over the central and eastern equatorial Pacific is below normal and the SST over the tropical NA is above normal. These findings are broadly consistent with previous studies (e.g., Shapiro and Goldenberg 1998; Sabbatelli and Mann 2007), although their focus is on TC counts.

Next we attempt to separate the ENSO effect from that of local SSTAs over the tropical NA, and we first explore the remote effect of ENSO by regressing high-frequency TC track density onto the Niño-3.4 index multiplied by -1 . (The negative values of the Niño-3.4 index are used to facilitate the comparison with the effect of tropical NA SST warming shown later.) In observations (Fig. 13a), La Niña with anomalously cold

SSTs over central and eastern equatorial Pacific favors above-normal TC track density almost everywhere in the NA basin, an effect most prominent over lower latitudes and the Gulf of Mexico. The variability explained by ENSO is around 5%–35%. HiRAM can generally simulate the effect by ENSO, but the simulated effect is relatively strong over the open ocean adjacent to the U.S. East Coast and relatively weak over the Gulf of Mexico and Caribbean Sea (Fig. 13c). Correcting the biases in the climatological TC track density, to some extent, improves the results (Fig. 13e).

Analyses of environmental variables suggest that the effect of ENSO on TC track density is achieved by affecting large-scale environmental factors, such as SLP and vertical wind shear (Fig. 14a), particularly over the low-latitude area, as has been extensively discussed in previous studies (e.g., Gray 1984).

We then perform the EOF analysis after removing ENSO-induced effect from the original high-frequency TC track density. The leading mode (mode H1*) again shows a basinwide change in both observations and HiRAM simulations (Figs. 13b,d,f). Compared to the

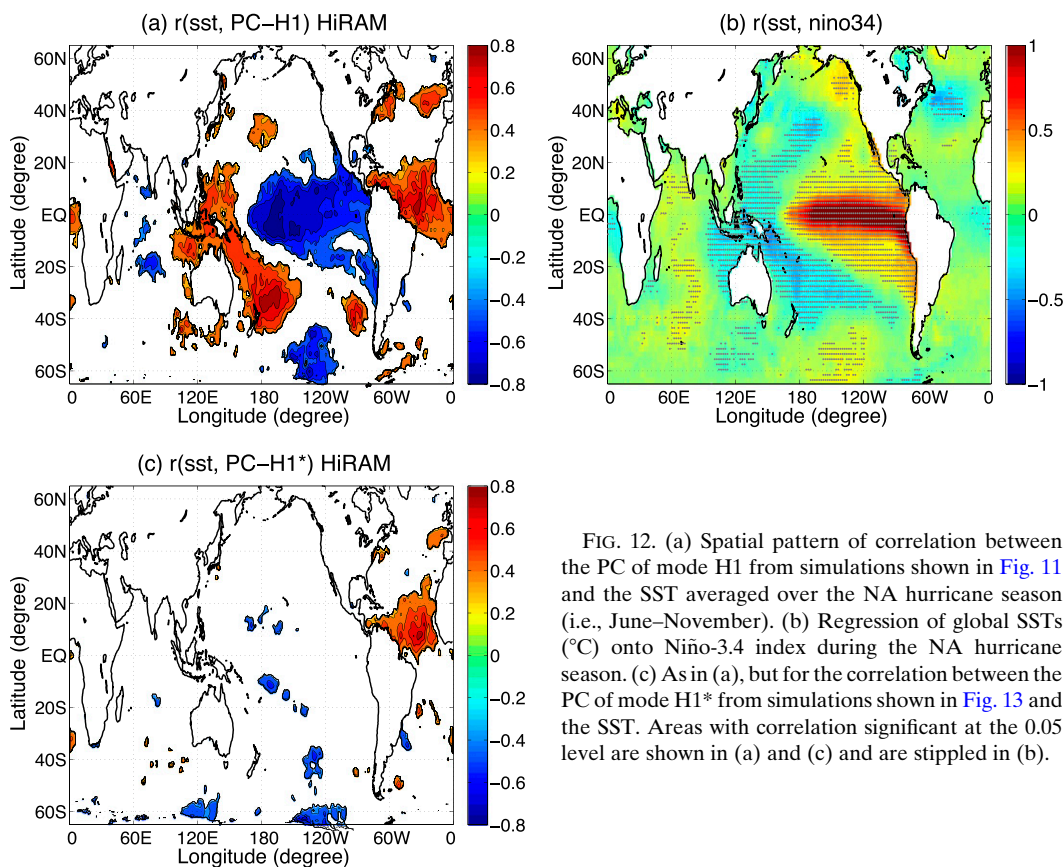


FIG. 12. (a) Spatial pattern of correlation between the PC of mode H1 from simulations shown in Fig. 11 and the SST averaged over the NA hurricane season (i.e., June–November). (b) Regression of global SSTs ($^{\circ}\text{C}$) onto Niño-3.4 index during the NA hurricane season. (c) As in (a), but for the correlation between the PC of mode H1* from simulations shown in Fig. 13 and the SST. Areas with correlation significant at the 0.05 level are shown in (a) and (c) and are stippled in (b).

ENSO effect, however, its amplitude is large over the higher-latitude region, particularly over the open ocean. Correlation of the corresponding PC with global SSTs suggests that this pattern is associated with SSTs over the tropical NA (Figs. 12c and 13g), supporting the hypothesis that SSTs in the central and eastern equatorial Pacific and those in the tropical NA force the NA TC track density independently.² When the SST over the MDR is warmer than normal, the SLP is below normal over the whole NA basin, the low-level vorticity is above normal, and the wind shear is weakened south of 20°N , producing a favorable environment for TC genesis and development (Fig. 14b).

Thus, it is clear that, during a La Niña event and/or when the tropical NA SST is warmer than normal, the whole NA basin experiences above-normal TC track density, although each effect has a strong spatial dependence (see also Kossin et al. 2010). This is similar to

the effect of tropical NA SSTs on TC track density on longer time scales, as discussed in the previous section.

Similar to the analysis for the low-frequency variability, we normalize the high-frequency component of TC track density by seasonal TC counts and then repeat the EOF analysis. Again, the observations (Figs. 15a,b) show two different oscillating modes (modes HN1 and HN2): one is southwest versus northeast, and the other is lower latitudes versus higher latitudes; they are similar to those for the low-frequency component (Figs. 7 and 9). In HiRAM simulations (Fig. 15c), these two modes appear to be combined, as indicated by the marginally significant correlation between the PC of mode HN1 in simulations and the PC of mode HN1 in observations ($r = 0.362$) and that between the PC of mode HN1 in simulations and the PC of mode HN2 in observations ($r = 0.345$) (Fig. 15d). The differences between the observed and simulated spatial patterns are associated with the biases in the simulated climatology of TC track density (Fig. 4).

Correlations of the PCs with global SSTs suggest that the first pattern (i.e., southwest versus northeast) is associated with ENSO while the second (i.e., lower latitudes versus higher latitudes) is linked to local tropical NA SSTs (not shown).

² It is worth noting that an El Niño (La Niña) event may induce warm (cold) SSTAs over the tropical NA during the winter and spring seasons, whose persistence may contribute to the state of tropical NA SSTAs during the hurricane season.

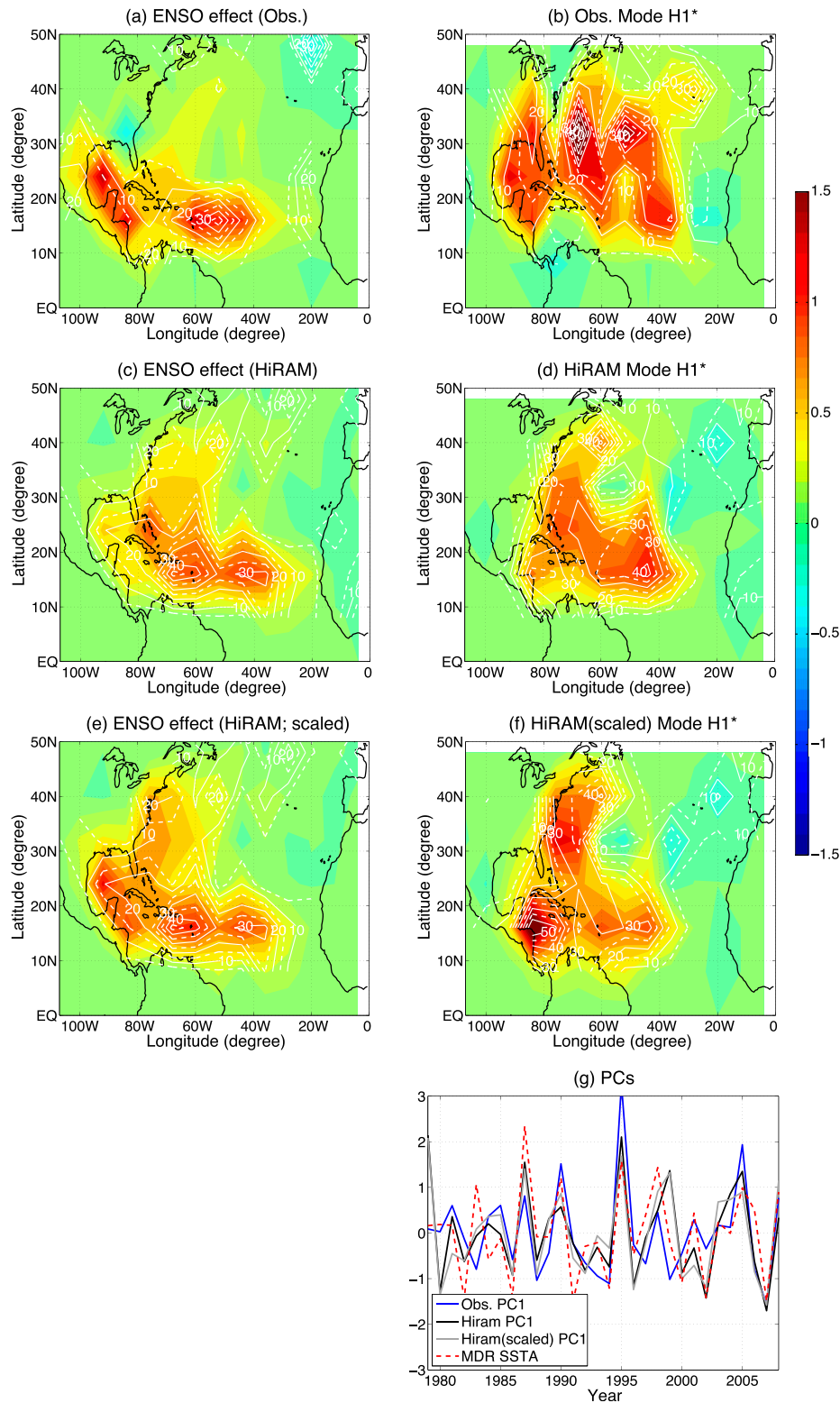


FIG. 13. (left) Regression onto the Niño-3.4 index multiplied by -1 of the high-pass-filtered TC track density (shading; days yr^{-1}) from (a) observations, (c) simulations, and (e) simulations after being normalized by the ratio of simulated climatology to observed climatology. (Thus, they show a condition induced by a La Niña event.) (b),(d),(f),(g) As in Fig. 11, but for the first leading mode of the high-pass-filtered TC track density after removing the contribution of ENSO (mode H1*). The normalized high-pass-filtered SSTA averaged over the MDR is also plotted in (g). White contours in (a)–(f) show the fraction of explained variance (%).

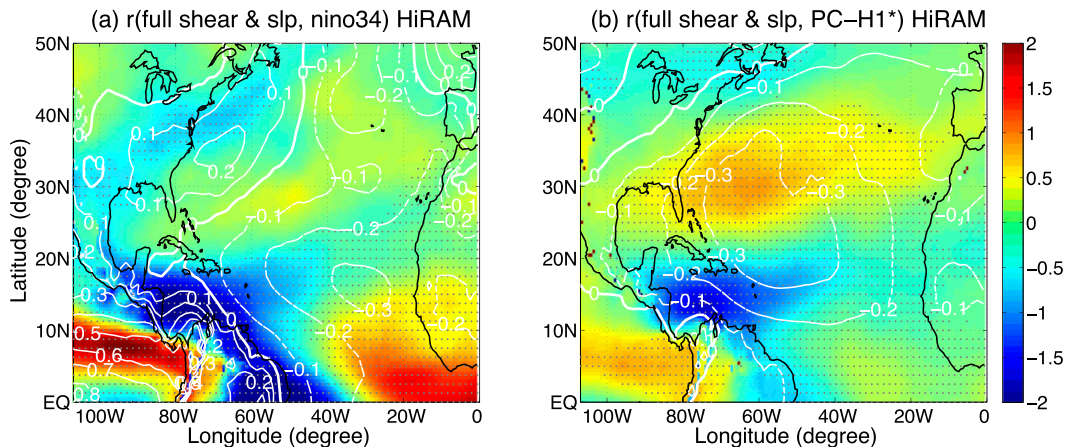


FIG. 14. Regression of the simulated high-pass-filtered vertical wind shear (shading; m s^{-1}) and SLP (contours; hPa) onto (a) the Niño-3.4 index multiplied by -1 and (b) the PC of mode H1* in simulations. Contour interval is 0.1 hPa.

6. Internal variability

As mentioned in section 2, we can partition TC track density at each grid in each simulation X into two components: an ensemble mean approximating the forced response³ X_F (this is what all the above analyses are based) and the departures from that mean X_I . To measure the importance of internal variability, we use the following metric, the signal-to-noise ratio:

$$R = \frac{\sigma_F}{\sigma_I}, \quad (1)$$

where σ_F is the standard deviation of the ensemble mean component X_F and σ_I , representing internal variability, is the standard deviation of the departures from the mean in all three ensemble members. A large value of R indicates that the internal variability is not as important as the forced response and hence there is less uncertainty.

Figure 16a shows the spatial distribution of the signal-to-noise ratio defined in Eq. (1). Large values can be found over the MDR and the open ocean adjacent to the continents and islands, suggesting the forced response in TC track density over the MDR (which is closely related to TC genesis) is stronger than over other regions. However, even the largest value is only around 1.1, indicating strong internal variability in TC track density over the whole NA basin. In contrast, the ratio is around 1.6 for both the NA TC counts and basin-integrated total TC days. This suggests the predictability of basinwide total TC counts or days are much higher than that of local

TC occurrence, posing a serious challenge to the prediction and projection of regional TC threats, although the prediction of seasonal total NA TC counts has significantly improved over recent years (e.g., Smith et al. 2010).

We further examine the internal variability in TC track density from a 20-yr experiment using the 50-km-resolution version HiRAM forced by repeating climatological SSTs. Figure 16b shows the ratio of the mean value of the track density to its standard deviation. [Note the definition of this ratio is different from the one defined in Eq. (1), making them quantitatively incomparable.] Again a small ratio denotes strong internal variability and correspondingly low predictability. The pattern of this ratio is consistent with the pattern of the signal-to-noise ratio shown in Fig. 16a: weaker internal variability and thus higher predictability over the MDR and the open ocean adjacent to the continents and islands. Interestingly, the corresponding ratio of the mean of the total TC counts or days to their respective standard deviation is around 4, which suggests again that basin-integrated metrics have a much higher predictability.

7. Summary and conclusions

This study has examined the interannual–decadal variability of tropical cyclone (TC) track density over the North Atlantic (NA) between 1979 and 2008 using TC best-track data from the National Hurricane Center and TC tracks detected from an ensemble of three simulations performed using a 25-km-resolution version of the High Resolution Atmospheric Model (HiRAM). Forced by observed sea surface temperatures (SSTs), HiRAM reproduces the observed temporal variations in seasonal counts of both TCs and hurricanes in the NA; it also generally captures the observed geographic distribution of the NA climatological TC track density, although there

³ A more strictly defined forced response can be obtained using the methodology described in Venzke et al. (1999) when the ensemble size is large enough (e.g., above 10). However, because we only have three simulations, we simply define the forced response as the ensemble mean of the three simulations.

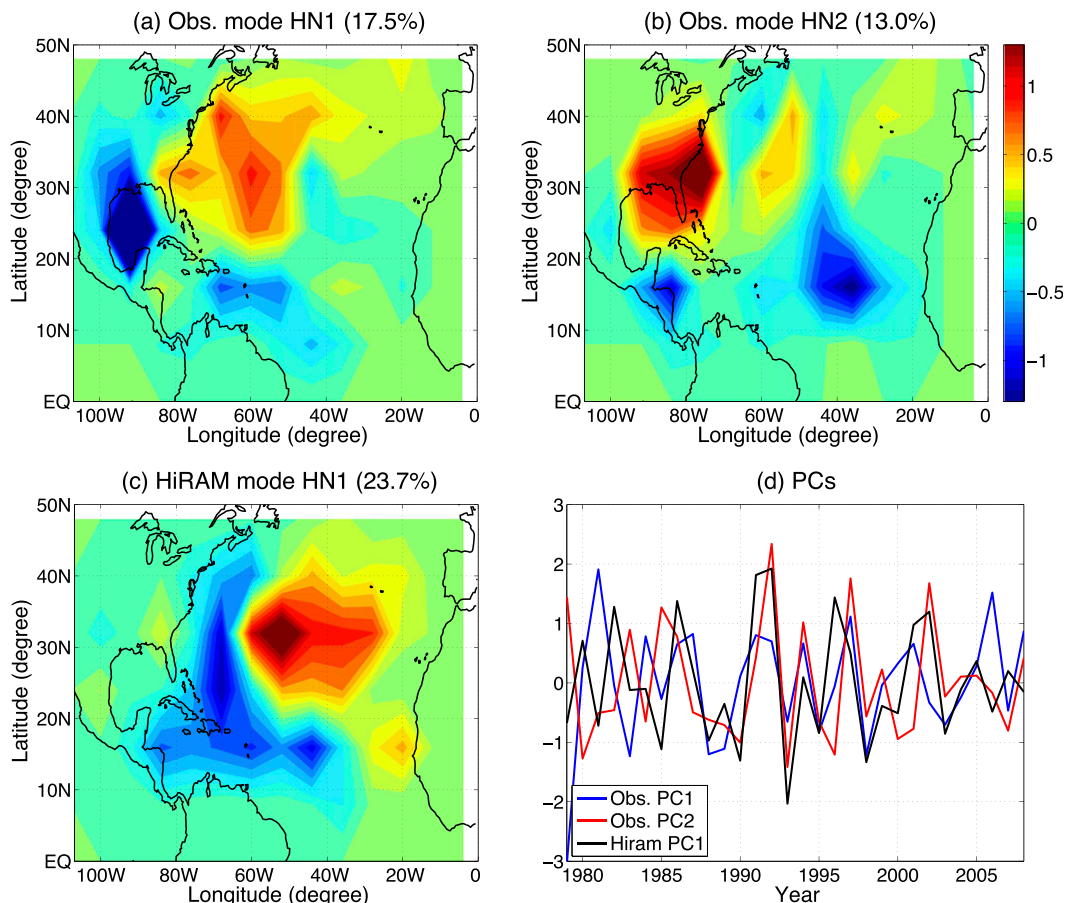


FIG. 15. (a) Spatial pattern of the first leading mode of the observed high-pass-filtered TC track density (mode HN1; days yr^{-1}) after being normalized using seasonal TC counts during the NA hurricane season. (b) As in (a), but for the second leading mode (mode HN2). (c) As in (a), but for the simulated TC track density. (d) Corresponding normalized PCs of modes HN1 (blue) and HN2 (red) in observations and mode HN1 in simulations (black).

are some systematic biases including underestimated density over the Gulf of Mexico and Caribbean Sea.

We partitioned TC track density into interannual and decadal components. Empirical orthogonal function (EOF) analyses show that on both time scales the variability of TC track density is dominated by a basinwide mode despite of some differences in the detailed spatial structure and the basinwide mode is strongly connected to variations in seasonal TC counts on both time scales.

Correlations of the principal component of the basinwide mode with global SSTs reveal that the decadal mode of NA TC track density is modulated by two SST dipole patterns: between the tropical NA and the tropical eastern North Pacific and between the tropical NA and the tropical South Atlantic. On interannual time scales, SST anomalies (SSTAs) over the central–eastern equatorial Pacific associated with El Niño–Southern Oscillation (ENSO) and over the tropical NA affect the NA TC activity: a La Niña state and anomalously warm tropical NA SSTs favor above-normal TC track density. These

two factors may not always act at the same time but can induce extreme TC activity when they work simultaneously. They affect TC activity by influencing environmental conditions in the atmosphere (e.g., low-level vorticity and vertical wind shear). In addition, the ENSO effect and the tropical NA SST effect have a strong spatial dependence: the former is more prominent over lower latitudes while the latter spreads over the whole NA.

To minimize the dominance of seasonal TC counts on the basinwide variability of TC track density and to examine the spatial variations, we normalized the seasonal track density at each grid point with seasonal TC counts and then repeated the EOF analysis. On decadal time scales, two spatial patterns emerge. One represents opposite variations in the contribution to basin-integrated TC track density between the following two regions: 1) the U.S. East Coast and midlatitude open ocean and 2) the Gulf of Mexico, Caribbean Sea, and—to a lesser extent—the main development region (MDR). This mode appears to be controlled by the North Atlantic

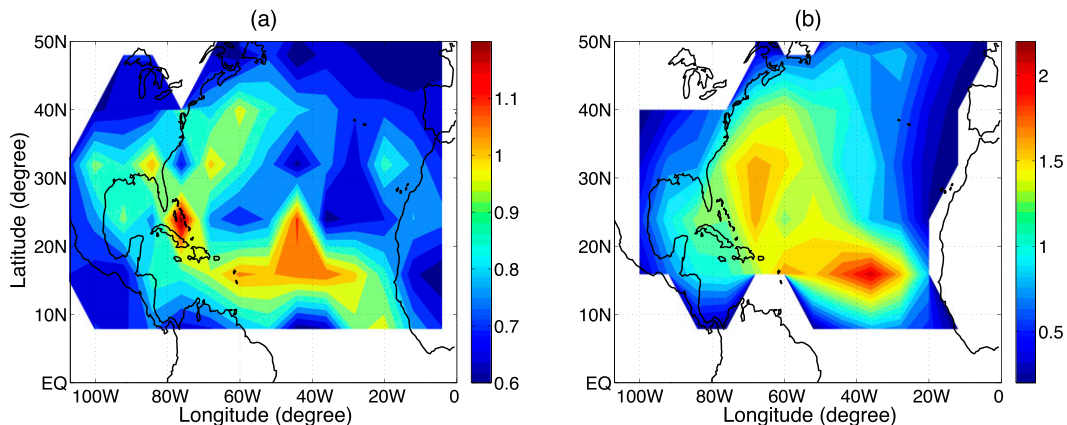


FIG. 16. (a) Signal-to-noise ratio calculated based on an ensemble of three members of the AMIP runs. (b) Ratio of the mean of the track density to its standard deviation in the climatological runs (see also section 2b).

Oscillation (NAO) condition during the preceding winter season with a positive NAO phase favoring higher proportion of TC track density over the East Coast and the midlatitude open ocean. This effect comes into play via the following mechanisms. First, the anomalous atmospheric circulation associated with a positive NAO phase during the winter season generates anomalously cold SSTs over both the mid–high-latitude and tropical NA. The negative SSTAs in the tropical NA then induce changes in atmospheric circulations across the Central America, which in turn produces anomalously warm SSTs over the tropical northeast Pacific. These SSTAs further strengthen the anomalous atmospheric circulations; affect both the position and strength of the subtropical high during the hurricane season; and generate below-normal TC activity over the Gulf of Mexico, Caribbean Sea, and MDR, leading to a reduced proportion of TC track density over these regions.

The second mode is an oscillation of the proportion of TC track density between low and midlatitudes in the meridional direction. This mode explains that the proportion of TC track density over the lower latitudes has increased since the mid-1980s, as reported by Kossin et al. (2010). This mode can be linked to a meridional contrast in SST between the tropical NA and the tropical South Atlantic: that is, the so-called Atlantic meridional mode. Analyses of atmospheric variables including low-level vorticity, midlevel vertical velocity, and vertical wind shear reveal that its effect on TC activity is achieved through a modulation of the position and strength of the NA intertropical convergence zone (ITCZ).

Two similar spatial patterns also exist for the normalized track density on interannual time scales, particularly in observations. In HiRAM simulations, these two modes are not well separated. These two modes are related to ENSO and local tropical NA SSTs,

respectively, as suggested by the correlation map of global SSTs.

Our analyses have shown that HiRAM well captures the observed variability of TC activity in various aspects on different time scales when subject to observed SST forcing, with important implications for predictability. When provided with an accurate prediction/projection in the pattern and magnitude of the SSTAs, HiRAM is able to provide useful information for not only the strength of basinwide TC activity but also the large-scale spatial distribution of track density (i.e., relative proportion of regional track density). Further improvements are needed, however, particularly for the simulation over the Gulf of Mexico and Caribbean Sea as HiRAM significantly underestimates TC activity over these areas. Also, we note that HiRAM underestimates the two extremely active seasons during the study period, 1995 and 2005 (Fig. 3). A rough look at the controlling modes on both decadal and interannual time scales (Figs. 5 and 13) indicates that the model may not be able to sufficiently capture the extreme TC occurrence that is related to the tropical NA SST warming. A more detailed attribution study will shed light on this.

The internal variability of the NA TC track density has also been explored based on HiRAM ensemble simulations. Calculations of the signal-to-noise ratio, defined as the ratio of the standard deviation of the ensemble mean to that of the deviations of the three ensemble members from the ensemble mean, show that internal variability is relatively weak in the MDR and along Caribbean islands but still generally comparable to the SST-forced variability. In contrast, the signal-to-noise ratio is much higher for total NA TC counts and basin-integrated TC days. This suggests that seasonal total TC counts are more predictable than local TC occurrence. Thus, on a seasonal basis, TC landfall—say, on the Gulf Coast and East Coast—appears stochastic and its accurate prediction is

difficult (e.g., Hall and Jewson 2007). This should be differentiated from the operational forecast of the path for a specific TC at a lead time of a few days, which has improved steadily in recent decades (e.g., Cangialosi and Franklin 2013). These findings also have important implications in the context of climate change: even if the multi-model ensemble can well project changes in total seasonal TC counts under global warming, it remains difficult to assess changes in local TC occurrence, particularly near the coast, where landfall TCs incur the greatest societal and economic impacts.

Acknowledgments. This work was funded by NSF Grant AGS-1305719 and NOAA Grant NA13OAR4310092. We thank Prof. Kerry Emanuel for sharing the compiled tropical cyclone best-track data, and we thank the editor and the anonymous reviewers for their comments that helped improve the manuscript.

REFERENCES

- Ballenzweig, E. M., 1959: Relation of long-period circulation anomalies to tropical storm formation and motion. *J. Meteor.*, **16**, 121–139, doi:10.1175/1520-0469(1959)016<0121:ROLPCA>2.0.CO;2.
- Bell, G. D., and M. Chelliah, 2006: Leading tropical modes associated with interannual and multidecadal fluctuations in North Atlantic hurricane activity. *J. Climate*, **19**, 590–612, doi:10.1175/JCLI3659.1.
- , and Coauthors, 2000: Climate assessment for 1999. *Bull. Amer. Meteor. Soc.*, **81** (6), S1–S50, doi:10.1175/1520-0477(2000)81[s1:CAF]2.0.CO;2.
- Cangialosi, J. P., and J. L. Franklin, 2013: 2012 National Hurricane Center forecast verification report. NOAA/National Hurricane Center Tech. Rep., 79 pp. [Available online at http://www.nhc.noaa.gov/verification/pdfs/Verification_2012.pdf.]
- Chang, P., and Coauthors, 2006: Climate fluctuations of tropical coupled systems—The role of ocean dynamics. *J. Climate*, **19**, 5122–5174, doi:10.1175/JCLI3903.1.
- Colbert, A. J., and B. J. Soden, 2012: Climatological variations in North Atlantic tropical cyclone tracks. *J. Climate*, **25**, 657–673, doi:10.1175/JCLI-D-11-00034.1.
- Daloz, A. S., F. Chauvin, K. Walsh, S. Lavender, D. Abbs, and F. Roux, 2012: The ability of general circulation models to simulate tropical cyclones and their precursors over the North Atlantic main development region. *Climate Dyn.*, **39**, 1559–1576, doi:10.1007/s00382-012-1290-7.
- DeMaria, M., J. A. Knaff, and B. H. Connell, 2001: A tropical cyclone genesis parameter for the tropical Atlantic. *Wea. Forecasting*, **16**, 219–233, doi:10.1175/1520-0434(2001)016<0219:ATCGPF>2.0.CO;2.
- Elsner, J. B., 2003: Tracking hurricanes. *Bull. Amer. Meteor. Soc.*, **84**, 353–356, doi:10.1175/BAMS-84-3-353.
- , K.-B. Liu, and B. Kocher, 2000: Spatial variations in major U.S. hurricane activity: Statistics and a physical mechanism. *J. Climate*, **13**, 2293–2305, doi:10.1175/1520-0442(2000)013<2293:SVIMUS>2.0.CO;2.
- Emanuel, K., 2001: Contribution of tropical cyclones to meridional heat transport by the oceans. *J. Geophys. Res.*, **106**, 14 771–14 781, doi:10.1029/2000JD900641.
- , 2005a: Increasing destructiveness of tropical cyclones over the past 30 years. *Nature*, **436**, 686–688, doi:10.1038/nature03906.
- , 2005b: Genesis and maintenance of “Mediterranean hurricanes.” *Adv. Geosci.*, **2**, 217–220, doi:10.5194/adgeo-2-217-2005.
- , 2007: Environmental factors affecting tropical cyclone power dissipation. *J. Climate*, **20**, 5497–5509, doi:10.1175/2007JCLI1571.1.
- , and A. Sobel, 2013: Response of tropical sea surface temperature, precipitation, and tropical cyclone-related variables to changes in global and local forcing. *J. Adv. Model. Earth Syst.*, **5**, 447–458, doi:10.1002/jame.20032.
- Fink, A. H., J. M. Schrage, and S. Kottlaus, 2010: On the potential causes of the nonstationary correlations between West African precipitation and Atlantic hurricane activity. *J. Climate*, **23**, 5437–5456, doi:10.1175/2010JCLI3356.1.
- George, J. E., and W. M. Gray, 1976: Tropical cyclone motion and surrounding parameter relationships. *J. Appl. Meteor.*, **15**, 1252–1264, doi:10.1175/1520-0450(1976)015<1252:TCMASP>2.0.CO;2.
- Goldenberg, S. B., and L. J. Shapiro, 1996: Physical mechanisms for the association of El Niño and West African rainfall with Atlantic major hurricane activity. *J. Climate*, **9**, 1169–1187, doi:10.1175/1520-0442(1996)009<1169:PMFTAO>2.0.CO;2.
- , C. W. Landsea, A. M. Mestas-Núñez, and W. M. Gray, 2001: The recent increase in Atlantic hurricane activity: Causes and implications. *Science*, **293**, 474–479, doi:10.1126/science.1060040.
- Gray, W. M., 1984: Atlantic seasonal hurricane frequency. Part I: El Niño and 30 mb Quasi-Biennial Oscillation influences. *Mon. Wea. Rev.*, **112**, 1649–1668, doi:10.1175/1520-0493(1984)112<1649:ASHFPI>2.0.CO;2.
- Griffies, S. M., and K. Bryan, 1997: A predictability study of simulated North Atlantic multidecadal variability. *Climate Dyn.*, **13**, 459–487, doi:10.1007/s003820050177.
- Hall, T. M., and S. Jewson, 2007: Statistical modelling of North Atlantic tropical cyclone tracks. *Tellus*, **59A**, 486–498, doi:10.1111/j.1600-0870.2007.00240.x.
- Harzallah, A., and R. Sadourny, 1995: Internal versus SST-forced atmospheric variability as simulated by an atmospheric general circulation model. *J. Climate*, **8**, 474–495, doi:10.1175/1520-0442(1995)008<0474:IVSFAV>2.0.CO;2.
- Holland, G. J., 1983: Tropical cyclone motion: Environmental interaction plus a beta effect. *J. Atmos. Sci.*, **40**, 328–342, doi:10.1175/1520-0469(1983)040<0328:TCMEIP>2.0.CO;2.
- , and P. J. Webster, 2007: Heightened tropical cyclone activity in the North Atlantic: Natural variability or climate trend? *Philos. Trans. Roy. Soc.*, **365A**, 2695–2716, doi:10.1098/rsta.2007.2083.
- Kanamitsu, M., W. Ebisuzaki, J. Woollen, S.-K. Yang, J. J. Hnilo, M. Fiorino, and G. L. Potter, 2002: NCEP–DOE AMIP-II Reanalysis (R-2). *Bull. Amer. Meteor. Soc.*, **83**, 1631–1643, doi:10.1175/BAMS-83-11-1631.
- Kimberlain, T. B., and J. B. Elsner, 1998: The 1995 and 1996 North Atlantic hurricane seasons: A return of the tropical-only hurricane. *J. Climate*, **11**, 2062–2069, doi:10.1175/1520-0442-11.8.2062.
- Klotzbach, P. J., 2011: El Niño–Southern Oscillation’s impact on Atlantic basin hurricanes and U.S. landfalls. *J. Climate*, **24**, 1252–1263, doi:10.1175/2010JCLI3799.1.
- , and W. M. Gray, 2008: Multidecadal variability in North Atlantic tropical cyclone activity. *J. Climate*, **21**, 3929–3935, doi:10.1175/2008JCLI2162.1.
- Knaff, J. A., 1997: Implications of summertime sea level pressure anomalies in the tropical Atlantic region. *J. Climate*, **10**, 789–804, doi:10.1175/1520-0442(1997)010<0789:IOSSLP>2.0.CO;2.

- Knutson, T. R., J. J. Sirutis, S. T. Garner, I. M. Held, and R. E. Tuleya, 2007: Simulation of the recent multidecadal increase of Atlantic hurricane activity using an 18-km-grid regional model. *Bull. Amer. Meteor. Soc.*, **88**, 1549–1565, doi:10.1175/BAMS-88-10-1549.
- Komaromi, W. A., 2013: An investigation of composite dropsonde profiles for developing and nondeveloping tropical waves during the 2010 PREDICT field campaign. *J. Atmos. Sci.*, **70**, 542–558, doi:10.1175/JAS-D-12-052.1.
- Korty, R. L., K. A. Emanuel, and J. R. Scott, 2008: Tropical cyclone-induced upper-ocean mixing and climate: Application to equable climates. *J. Climate*, **21**, 638–654, doi:10.1175/2007JCLI1659.1.
- Kossin, J. P., and D. J. Vimont, 2007: A more general framework for understanding Atlantic hurricane variability and trends. *Bull. Amer. Meteor. Soc.*, **88**, 1767–1781, doi:10.1175/BAMS-88-11-1767.
- , S. J. Camargo, and M. Sitkowski, 2010: Climate modulation of North Atlantic hurricane tracks. *J. Climate*, **23**, 3057–3076, doi:10.1175/2010JCLI3497.1.
- Landsea, C. W., and W. M. Gray, 1992: The strong association between western Sahelian monsoon rainfall and intense Atlantic hurricanes. *J. Climate*, **5**, 435–453, doi:10.1175/1520-0442(1992)005<0435:TSABWS>2.0.CO;2.
- , R. A. Pielke Jr., A. M. Mestas-Nuñez, and J. A. Knaff, 1999: Atlantic Basin hurricanes: Indices of climatic changes. *Climatic Change*, **42**, 89–129, doi:10.1023/A:1005416332322.
- McAdie, C. J., C. W. Landsea, C. J. Neumann, J. E. David, E. S. Blake, and G. R. Hammer, 2009: *Tropical Cyclones of the North Atlantic Ocean, 1851–2006*. Historical Climatology Series, Vol. 6-2, NOAA, 238 pp.
- McBride, J. L., and R. Zehr, 1981: Observational analysis of tropical cyclone formation. Part II: Comparison of non-developing versus developing systems. *J. Atmos. Sci.*, **38**, 1132–1151, doi:10.1175/1520-0469(1981)038<1132:OAOTCF>2.0.CO;2.
- Mei, W., F. Primeau, J. C. McWilliams, and C. Pasquero, 2013: Sea surface height evidence for long-term warming effects of tropical cyclones on the ocean. *Proc. Natl. Acad. Sci. USA*, **110**, 15 207–15 210, doi:10.1073/pnas.1306753110.
- Merlis, T. M., M. Zhao, and I. M. Held, 2013: The sensitivity of hurricane frequency to ITCZ changes and radiatively forced warming in aquaplanet simulations. *Geophys. Res. Lett.*, **40**, 4109–4114, doi:10.1002/grl.50680.
- Nolan, D. S., and E. D. Rappin, 2008: Increased sensitivity of tropical cyclogenesis to wind shear in higher SST environments. *Geophys. Res. Lett.*, **35**, L14805, doi:10.1029/2008GL034147.
- Pielke, R. A., Jr., and C. W. Landsea, 1998: Normalized hurricane damages in the United States: 1925–95. *Wea. Forecasting*, **13**, 621–631, doi:10.1175/1520-0434(1998)013<0621:NHDITU>2.0.CO;2.
- , J. Gratz, C. W. Landsea, D. Collins, M. A. Saunders, and R. Musulin, 2008: Normalized hurricane damage in the United States: 1900–2005. *Nat. Hazards Rev.*, **9**, 29–42, doi:10.1061/(ASCE)1527-6988(2008)9:1(29).
- Raymond, D. J., and S. L. Sessions, 2007: Evolution of convection during tropical cyclogenesis. *Geophys. Res. Lett.*, **34**, L06811, doi:10.1029/2006GL028607.
- Rayner, N. A., D. E. Parker, E. B. Horton, C. K. Folland, L. V. Alexander, D. P. Rowell, E. C. Kent, and A. Kaplan, 2003: Global analyses of sea surface temperature, sea ice, and night marine air temperature since the late nineteenth century. *J. Geophys. Res.*, **108**, 4407, doi:10.1029/2002JD002670.
- Sabbatelli, T. A., and M. E. Mann, 2007: The influence of climate state variables on Atlantic tropical cyclone occurrence rates. *J. Geophys. Res.*, **112**, D17114, doi:10.1029/2007JD008385.
- Shapiro, L. J., and S. B. Goldenberg, 1998: Atlantic sea surface temperatures and tropical cyclone formation. *J. Climate*, **11**, 578–590, doi:10.1175/1520-0442(1998)011<0578:ASSTAT>2.0.CO;2.
- Simpson, J., E. Ritchie, G. J. Holland, J. Halverson, and S. Stewart, 1997: Mesoscale interactions in tropical cyclone genesis. *Mon. Wea. Rev.*, **125**, 2643–2661, doi:10.1175/1520-0493(1997)125<2643:MIITCG>2.0.CO;2.
- Smirnov, D., and D. J. Vimont, 2011: Variability of the Atlantic meridional mode during the Atlantic hurricane season. *J. Climate*, **24**, 1409–1424, doi:10.1175/2010JCLI3549.1.
- Smith, D. M., R. Eade, N. J. Dunstone, D. Fereday, J. M. Murphy, H. Pohlmann, and A. A. Scaife, 2010: Skilful multi-year predictions of Atlantic hurricane frequency. *Nat. Geosci.*, **3**, 846–849, doi:10.1038/ngeo1004.
- Smith, R. K., and M. T. Montgomery, 2012: Observations of the convective environment in developing and non-developing tropical disturbances. *Quart. J. Roy. Meteor. Soc.*, **138**, 1721–1739, doi:10.1002/qj.1910.
- Srifer, R. L., and M. Huber, 2007: Observational evidence for an ocean heat pump induced by tropical cyclones. *Nature*, **447**, 577–580, doi:10.1038/nature05785.
- Sutton, R. T., and D. L. R. Hodson, 2007: Climate response to basin-scale warming and cooling of the North Atlantic Ocean. *J. Climate*, **20**, 891–907, doi:10.1175/JCLI4038.1.
- Venzke, S., M. R. Allen, R. T. Sutton, and D. P. Rowell, 1999: The atmospheric response over the North Atlantic to decadal changes in sea surface temperature. *J. Climate*, **12**, 2562–2584, doi:10.1175/1520-0442(1999)012<2562:TAROTN>2.0.CO;2.
- Vimont, D. J., and J. P. Kossin, 2007: The Atlantic meridional mode and hurricane activity. *Geophys. Res. Lett.*, **34**, L07709, doi:10.1029/2007GL029683.
- Vitart, F., and J. L. Anderson, 2001: Sensitivity of Atlantic tropical storm frequency to ENSO and interdecadal variability of SSTs in an ensemble of AGCM integrations. *J. Climate*, **14**, 533–545, doi:10.1175/1520-0442(2001)014<0533:SOATSF>2.0.CO;2.
- Wang, C., H. Liu, S.-K. Lee, and R. Atlas, 2011: Impact of the Atlantic warm pool on United States landfalling hurricanes. *Geophys. Res. Lett.*, **38**, L19702, doi:10.1029/2011GL049265.
- Wang, Z., 2012: Thermodynamic aspects of tropical cyclone formation. *J. Atmos. Sci.*, **69**, 2433–2451, doi:10.1175/JAS-D-11-0298.1.
- Xie, L., T. Yan, and L. Pietrafesa, 2005a: The effect of Atlantic sea surface temperature dipole mode on hurricanes: Implications for the 2004 Atlantic hurricane season. *Geophys. Res. Lett.*, **32**, L03701, doi:10.1029/2004GL021702.
- , —, —, J. M. Morrison, and T. Karl, 2005b: Climatology and interannual variability of North Atlantic hurricane tracks. *J. Climate*, **18**, 5370–5381, doi:10.1175/JCLI3560.1.
- Zhang, R., and T. L. Delworth, 2005: Simulated tropical response to a substantial weakening of the Atlantic thermohaline circulation. *J. Climate*, **18**, 1853–1860, doi:10.1175/JCLI3460.1.
- Zhao, M., I. M. Held, S.-J. Lin, and G. A. Vecchi, 2009: Simulations of global hurricane climatology, interannual variability, and response to global warming using a 50-km resolution GCM. *J. Climate*, **22**, 6653–6678, doi:10.1175/2009JCLI3049.1.
- , —, and —, 2012: Some counterintuitive dependencies of tropical cyclone frequency on parameters in a GCM. *J. Atmos. Sci.*, **69**, 2272–2283, doi:10.1175/JAS-D-11-0238.1.